# Robust Voltage Control Considering Uncertainties of Renewable Energies and Loads via Improved Generative Adversarial Network

Qianyu Zhao, Wenlong Liao, Shouxiang Wang, and Jayakrishnan Radhakrishna Pillai

***Abstract*—The fluctuation of output power of renewable energies and loads brings challenges to the scheduling and operation of the distribution network. In this paper, a robust voltage control model is proposed to cope with the uncertainties of renewable energies and loads based on an improved generative adversarial network (IGAN). Firstly, both real and predicted data are used to train the IGAN consisting of a discriminator and a generator. The noises sampled from the Gaussian distribution are fed to the generator to generate a large number of scenarios that are utilized for robust voltage control after scenario reduction. Then, a new improved wolf pack algorithm (IWPA) is presented to solve the formulated robust voltage control model, since the accuracy of the solutions obtained by traditional methods is limited. The simulation results show that the IGAN can accurately capture the probability distribution characteristics and dynamic nonlinear characteristics of renewable energies and loads, which makes the scenarios generated by IGAN more suitable for robust voltage control than those generated by traditional methods. Furthermore, IWPA has a better performance than traditional methods in terms of convergence speed, accuracy, and stability for robust voltage control.**

***Index Terms*—Robust voltage control, uncertainty, generative adversarial network, wolf pack algorithm.**

## I. Introduction

In recent years, the penetration rates of electric vehicles and renewable energies into the distribution network have increased rapidly, and their fluctuations have brought great challenges to the planning and operation of the distribution network [1]. For example, the integration of wind farms may cause the voltages of nodes in the distribution network to exceed the limit. Hence, it is of great significance for the distribution network to consider the uncertainty of renewable energies and loads for scheduling the distribution network.

The traditional methods for voltage control belong to the deterministic voltage control (DVC) model, which does not consider the uncertainties of renewable energies and loads [2]. On one hand, the real-time measurement is often insufficient in the distribution network, and the state estimation depends on the pseudo measurement data, which leads to a large error in the power load estimation [3]. On the other hand, the fluctuation of wind speed and light intensity leads to the uncertainties of output power of renewable generation units. In this case, the voltage control strategy of the DVC model may not be safe for the distribution network on the high penetration of distributed generation units [4]. Therefore, the power operation and planning department should take the uncertainties of renewable energies and loads into account when making decisions for voltage control.

Currently, the mainstream methods dealing with uncertainties of renewable energies and loads include stochastic optimization, fuzzy optimization, interval optimization, and robust optimization [5], [6]. For example, the radial basis function neural network and the fuzzy unscented transform are combined to calculate probabilistic power flow in microgrid including electric vehicles, wind, and solar distributed energy resources [7], [8]. To obtain the optimal bidding strategies for wind farms and hydro stations in a power generation company, the interval optimization is used in [9]. In general, the interval, fuzzy and stochastic optimization methods cannot assure that the obtained strategies can be always feasible for any possible combination of renewable energies and loads [10]. Specifically, when the real power loads are large and the output power of wind farms is small, the control strategy of these methods cannot guarantee that the node voltages in the distribution network are not lower than the limit. By contrast, robust optimization attempts to find a conservative strategy that can guarantee the safe operation of the distribution network in any scenario at the cost of the economy. Now, the robust optimization is receiving more and more attention in various fields of distribution network operation [11].

To present the uncertainties of renewable energies and loads, the scenario generation technology is often used to generate a scenario set for robust optimization. Most of the previous works use explicit density models (e. g., copula function, moment matching technique, and generalized dynamic factor methods) to generate the scenario set through

Manuscript received: April 14, 2020; accepted: September 4, 2020. Date of CrossCheck: September 4, 2020. Date of online publication: November 26, 2020.

This work was supported by the Science and Technology Project of State Grid Corporation of China.



Q. Zhao, W. Liao (corresponding author), and S. Wang are with the Key Laboratory of Smart Grid of Ministry of Education and Tianjin Key Laboratory of Power System Simulation and Control, Tianjin University, Tianjin, China (e-mail: zhaoqianyu@tju.edu.cn; wenlongliao@cau.edu.cn; sxwang@tju.edu.cn).

J. Pillai is with the Department of Energy Technology, Aalborg University, Aalborg, Denmark (e-mail: jrp@et.aau.dk).

DOI: 10.35833/MPCE.2020.000210

fitting and sampling probability distribution or empirical distribution [12]. However, these methods need to artificially assume the distribution function, which is difficult to be described accurately by a mathematical formula. In addition, the spatial-temporal characteristics of loads and renewable energies are difficult to be accurately fitted by second-order statistical results [13]. In recent years, some deep learning based methods such as the variational automatic encoder (VAE) and generative adversarial network (GAN) have also been used for scenario generation [14], [15]. These methods belong to the implicit density model, which does not need to explicitly fit the probability distribution or empirical distribution, and can capture the dynamic nonlinear characteristics of renewable energies and loads through training and sampling. However, the performance of VAE is worse than that of GAN, because it does not use the adversarial for training. The shortcomings of GAN such as vanishing gradients and exploding gradients problem still exist and these problems lead to poor quality of generated data [16].

From the standpoint of solution, the existing methods can be summarized into two categories, including mathematical programming algorithms and heuristic algorithms. The mathematical programming algorithms mainly include nonlinear programming, linear programming, and dynamic programming [17]. These methods have been widely used in the various fields of power system optimization because of their low complexity and fast computing speed [18]. Nevertheless, it is difficult for them to solve nonlinear and high-dimensional robust voltage optimization problems accurately [19]. The heuristic algorithms mainly include the genetic algorithm (GA), fireworks algorithm (FWA), artificial bee colony (ABC) algorithm, and imperialist competitive algorithm (ICA) [20]. For example, a parametric GA is proposed to find the optimal spatial distribution of renewable units in [21]. To minimize the total operation cost of material handling, a novel discrete ICA with a priority rule based heuristic is designed in [22]. While in [23], the ABC is utilized to effectively generate a set of Pareto solutions for a dual-objective disassembly optimization problem. In general, these methods are extremely suitable for treating discontinuous and non-convex problems. However, their performances are easily affected by the parameters, and they are easy to get the local optimal solution with limited accuracy [10]. Therefore, a new method is needed to solve the nonlinear robust optimization problem.

Although previous works have provided a lot of important insights for robust voltage control (RVC), there are still many problems to be addressed. For example, a model-free method without vanishing gradients needs to be designed to capture the uncertainties of renewable energies and loads, and a high-efficiency solution method is needed for robust optimization. To solve these problems, a new approach for RVC considering uncertainties of loads and renewable energies via an improved generative adversarial network (IGAN) is proposed in this paper. The key contributions can be summarized as follows.

1) An IGAN is designed to improve the quality of the generated data and the stability of the training process according to the characteristics of renewable energies and loads, because the traditional implicit density models have the problems of vanishing gradient or poor quality of generated data. Unlike the explicit density models, IGAN does not need to artificially assume the probability distributions of renewable energies and loads, and generates the scenarios for different objects by adjusting the structure and parameters. Moreover, the generated scenarios can accurately capture the probability distribution characteristics and dynamic nonlinear characteristics of renewable energies and loads, which make the scenarios generated by IGAN more suitable for the RVC model than those generated by traditional methods such as VAE.

2) The RVC model is proposed to fully take comprehensive uncertainties of loads and renewable energies into account. The differences between DVC and RVC model in voltage and power losses are demonstrated.

3) Due to the limited accuracy of the traditional methods for solving the RVC model, a new improved wolf pack algorithm (IWPA) is proposed. The simulation results show that the new method has better accuracy and stability than those of traditional methods such as GA, ABC, and ICA.

The remainder of this paper is organized as follows. Section II proposes the RVC model. Section III presents the IGAN for scenario generation. In Section IV, the IWPA is designed to solve the RVC model. The effectiveness of the proposed approaches is verified by simulation in Section V. Section VI shows the discussion. Section VII shows the conclusions and future work.

## II. RVC Model

### *A. Deterministic Model Description*

In the optimal dispatching model of distribution network, the control variables mainly include the tap position of on-load tap changer (OLTC), shunt capacitors, static var compensator (SVC), and reactive power of distributed generations. The objective function is to minimize the power loss of the distribution network, and its mathematical formula is as follows:

$$\min f_{loss} = \sum_{l=1}^{N} R_l \frac{P_l^2 + Q_l^2}{U_l^2} \tag{1}$$

where $f_{loss}$ is the power loss of the distribution network; $R_l$ is the resistance of the $l^{\text{th}}$ branch; $N$ is the total number of branches in the distribution network; $U_l$ is the voltage amplitude of the $l^{\text{th}}$ branch; and $P_l$ and $Q_l$ are the real power and reactive power flowing through the end of the $l^{\text{th}}$ branch, respectively.

The constraints of this optimization model mainly include:

1) Network power balance

$$\begin{cases} P_i = U_i \sum_{j=1}^{n} U_j \left( G_{ij} \cos \delta_{ij} + B_{ij} \sin \delta_{ij} \right) \\ Q_i = U_i \sum_{j=1}^{n} U_j \left( G_{ij} \sin \delta_{ij} - B_{ij} \cos \delta_{ij} \right) \end{cases} \tag{2}$$

where $n$ is the total number of nodes; $G_{ij}$ and $B_{ij}$ are the conductance and susceptance of the branch, respectively; and $\delta_{ij}$ is the phase difference of the voltage between the $i^{\text{th}}$ node and $j^{\text{th}}$ node.

2) Voltage and current limits

$$\begin{cases} U_{i,\min} \le U_i \le U_{i,\max} \\ 0 \le I_l \le I_{l,\max} \end{cases} \tag{3}$$

where $U_{i,\min}$ is the lower limit for the $i^{\text{th}}$ node, which is equal to 0.95 for generic nodes and 0.9 for OLTC secondary nodes; $U_{i,\max}$ is the upper limit for the $i^{\text{th}}$ node, which is equal to 1.05 for generic nodes and 1.1 for OLTC secondary nodes [4]; and $I_{l,\max}$ is the upper limit of the current in the $l^{\text{th}}$ branch.

3) OLTC and shunt capacitors limits

$$\begin{cases} T_{k,\min} \le T_k \le T_{k,\max} \\ 0 \le Q_{ci} \le Q_{ci,\max} \end{cases} \tag{4}$$

where $T_{k,\min}$ and $T_{k,\max}$ are the minimum and maximum values of the OLTC position, respectively; and $Q_{ci,\max}$ is the maximum value of the shunt capacitors.

4) SVC and distributed generation limits

$$\begin{cases} Q_{i,\text{SVC},\min} \le Q_{i,\text{SVC}} \le Q_{i,\text{SVC},\max} \\ Q_{i,\text{DG},\min} \le Q_{i,\text{DG}} \le Q_{i,\text{DG},\max} \end{cases} \tag{5}$$

where $Q_{i,\text{SVC},\min}$ and $Q_{i,\text{SVC},\max}$ are the minimum and maximum reactive power of SVC, respectively; and $Q_{i,\text{DG},\min}$ and $Q_{i,\text{DG},\max}$ are the minimum and maximum reactive power of distributed generations, respectively. Normally, these distributed generations are PQ units and not PV units. Therefore, the real power of distributed generations is assumed to be fixed and the reactive power is the control variables in this paper.

### B. Robust Model Description

The main components in the robust voltage control are the scenario generation and deterministic optimization. Firstly, the real and the day-ahead predicted data are used to train IGAN. After training, the generator of IGAN generates a large number of scenarios for renewable energies and loads. In order to reduce the complexity of the algorithm, $K$-means is used to reduce the number of similar scenarios. Then, IWPA is used to get extreme scenarios. Finally, IWPA is used to find the optimal solution of the DVC model in the normal scenario, and the optimal solution needs to ensure that the voltages do not exceed the limit in extreme scenarios.

The amplitude of the voltage is an important index to evaluate the reliability of the distribution network. In this paper, the extreme scenario is defined by the voltage amplitude of nodes, and its mathematical formula is:

$$\max f_U = \max \left| U_i - U_{\text{N}} \right| \quad i = 1, 2, \ldots, n \tag{6}$$

where $U_{\text{N}}$ is the rated voltage in the distribution network. Obviously, (6) includes two kinds of extreme scenarios: ① when the load is very large and the output power of renewable sources is very small, the voltage amplitude may be less than the lower limit; ② when the load is very small and the output power of renewable sources is very large, the voltage amplitude may exceed the upper limit.

IWPA is used to find the extreme scenarios from those generated by IGAN. The control variables are the scenarios of renewable energies and loads, and the objective function is (6).

## III. Generation and Reduction for Scenarios

### A. Traditional GAN

GAN is a kind of deep generative network consisting of a generator and discriminator. The generator contests with the discriminator in a game, and they can be regarded as counterfeiters and money detectors [24] - [26]. The generator is considered as a counterfeiter, whose purpose is to generate counterfeit currency that cannot be recognized by the money detector. The discriminator is considered as a money detector, whose purpose is to identify the counterfeit money made by counterfeiters as much as possible. After training, the generator can produce particularly realistic counterfeit currency, while the probability that the discriminator identifies the counterfeit currency is 50%.

Specifically, the framework of scenario generation for renewable energies and loads based on GAN is shown in Fig. 1. The generator learns the features of the historical samples from the training set to generate new data. The discriminator is a classifier to judge whether the input sample is true or fake. When the discriminator of GAN is trained, the parameters of the generator are fixed. Firstly, the loss function of the discriminator is calculated after the samples are input into the discriminator. Then, the parameters of the discriminator are updated by the back propagation algorithm [27]. The loss function of the discriminator is:

$$\max E_{X\sim P_{data}(x)}\left(\lg D(x)\right) + E_{Z\sim P_Z(z)}\left(\lg\left(1 - D\left(G(z)\right)\right)\right) \tag{7}$$

where $X\sim P_{data}(x)$ is the probability distribution of real samples; $Z\sim P_Z(z)$ is a simple distribution (e.g., Gaussian distribution in this paper) that is used to obtain random noises; $D(x)$ is a value that ranges from 0 to 1, indicating the probability that the input sample is true; and $\lg(1-D(G(z)))$ is the probability that the discriminator judges the generated sample is fake. In the training process, the goal of the discriminator is to make the objective function as large as possible.

Similarly, when the generator of GAN is trained, the parameters of the discriminator are fixed. Firstly, the generator produces new samples that are used to calculate the loss function of the generator. Then, the parameters of the generator are updated by back propagation algorithm. The goal of the generator is to generate samples that closely resemble to real samples. The loss function of the generator is opposite to that of the discriminator. Its mathematical formula is:

$$\min \max E_{X\sim P_{data}(x)}\left(\lg D(x)\right) + E_{Z\sim P_Z(z)}\left(\lg\left(1 - D\left(G(z)\right)\right)\right) \tag{8}$$

After multiple cross-training, the GAN will converge to the Nash equilibrium.

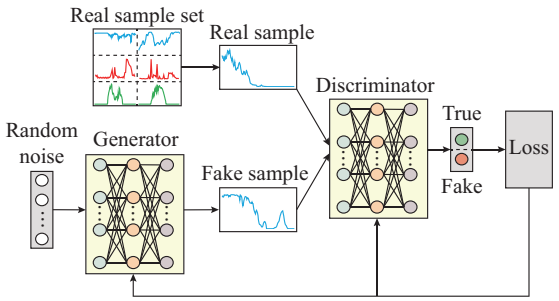


Fig. 1. Framework of GAN for scenario generation.

### B. Improved GAN

Convolutional neural network (CNN) is a kind of feed-forward neural network with convolution operation. Its appearance has greatly accelerated the development of artificial intelligence. CNN has been widely used in stability assessment, target detection, semantic segmentation, fault diagnosis, and other fields due to its powerful feature extraction ability [28]. In this paper, CNN is used to improve the quality of the generated data. The details of the change include the following four aspects.

1) To improve the ability of feature extraction [29], the dense layers in the hidden layer are replaced by convolutional layers.

2) All pooling layers in the generator are replaced by fractional-strided convolutions. Similarly, all pooling layers in the discriminator are replaced by strided convolutions. In this case, the network can learn its own spatial sampling [30].

3) The batch normalization can stabilize the learning process by mapping the samples to each unit to have unit variance and zero mean, which can accelerate the convergence of the network and avoid over-fitting [31]. Therefore, the batch normalization will be applied to the generator and the discriminator.

4) In the generator, the rectified linear unit (ReLU) is used as the activate function for all layers except the output layer that uses the tanh function, since these activation functions can help the model learn the probability distribution of real samples more quickly. In the discriminator, the previous work indicates that the leaky rectified activation performs well [32]. Thus, the LeakyReLU is used as the activate function for all layers.

It can be seen from (8) that the loss of sigmoid cross-entropy is used as the loss function for the discriminator in the traditional GAN. The existing literature shows that this loss function causes the vanishing gradient problem, since the generated samples are on the right side of the decision boundary, but they are still far from the true samples [16]. To solve these problems, the least squares are utilized as the loss function for the discriminator. In this case, the generated samples move towards the decision boundary, since the least squares loss function penalizes the samples. The loss function of the improved GAN is:

$$\min \frac{1}{2}E_{X\sim P_{data}(x)}\left(\left(D(x)-b\right)^2\right)+\frac{1}{2}E_{Z\sim P_Z(z)}\left(\left(D\left(G(z)\right)-a\right)^2\right) \quad (9)$$

$$\min \frac{1}{2}E_{Z\sim P_Z(z)}\left(\left(D\left(G(z)\right)-c\right)^2\right) \quad (10)$$

where parameters need to satisfy this property of $b-a=2$ and $b-c=1$ based on the suggestions of the existing literature [13]. In this paper, the parameters are set as: $a=-1$, $b=1$, and $c=0$.

Based on the above description, the steps of scenario generation by IGAN are as follows.

*Step 1*: before input real and predicted data into IGAN, the samples need to be normalized, and otherwise the loss function may not converge. In this paper, the min-max normalization method is used to transfer the input data into the values that range from 0 to 1.

*Step 2*: the $m$ random noises are obtained by sampling from the prior distribution $Z\sim P_Z(z)$. In each round of training, the parameters of the discriminator will be updated $k_1$ times with the back propagation algorithm.

*Step 3*: the $m$ samples are obtained by feeding the $m$ random noises to the generator.

*Step 4*: the stochastic gradient values of the discriminator are calculated to update the parameters of the discriminator. If the number of updates does not exceed $k_1$, return to *Step 3* to continue to update the parameters of the discriminator. The gradient of the discriminator is:

$$\nabla_\theta \frac{1}{m}\sum_{t=1}^{m}\left[\frac{1}{2}\left(D\left(x^t\right)-1\right)^2+\frac{1}{2}\left(D\left(G\left(z^t\right)\right)+1\right)^2\right] \quad (11)$$

*Step 5*: the $m$ random noises are obtained by sampling from the prior distribution $Z\sim P_Z(z)$. The stochastic gradient of the generator is calculated to update the parameters of the generator. The stochastic gradient of the generator is:

$$\nabla_\varnothing \frac{1}{m}\sum_{t=1}^{m}\frac{1}{2}D\left(G\left(z^t\right)\right)^2 \quad (12)$$

*Step 6*: return to *Step 2* unless the IGAN reaches the preset maximum number of iterations.

*Step 7*: after the training, the random noises are obtained by sampling from the prior distribution $Z\sim P_Z(z)$ as input data of the generator to get the scenarios of renewable energies and loads.

## IV. Wolf Pack Algorithm

### A. Traditional Wolf Pack Algorithm

The efficiency and accuracy of most traditional heuristic algorithms are not good and easy enough to get the local optimal solution [10]. To solve this problem, the behaviors of the wolves is analyzed and a wolf pack algorithm (WPA) is proposed [33]. The simulation results show that the WPA has better global optimization ability and stronger robustness than those of the traditional heuristic algorithm, especially for high-dimensional optimization [34]. This paper will try to apply the WPA to solve the RVC model. Furthermore, since the RVC model requires the heuristic algorithm to have excellent stability and high accuracy, two strategies are proposed to improve the traditional WPA, which includes five steps as follows.

*Step 1*: initialization of wolf pack. It assumes that $A$ is the number of variables that range from 0 to 1. The wolf pack

consists of $H$ wolves, each of which has $A$ random numbers between 0 and 1. The objective function of each wolf is calculated, and the wolves are sorted according to the order of the objective function from good to bad. The wolf with the best objective function value is selected as the lead wolf.

*Step 2*: scouting behavior. The former $L$ wolves are regarded as the scout wolves except for the lead wolf. The scout wolves select $h$ directions around to search the solution. If the near solution is better than the current solution, the scout wolves will move to the new position. If the searching times of the scout wolf reach the maximum number (the maximum number is 7 in this paper) or the solution of new position $f_{new,loss}$ is better than that of the old position $f_{old,loss}$, the searching will stop.

*Step 3*: calling behavior. Except for the lead wolf and scout wolves, the rest are the ferocious wolves. The lead wolf will summon the ferocious wolves to gather the solution around it. Specifically, the process of calling behavior is as follows. Firstly, $k$ positions between 1 and $A$ are randomly selected. Secondly, the variables of ferocious wolves are replaced with the variables of the lead wolf in selected positions. Thirdly, if the objective function of the wolf in the new position is better than that in the old position, it will accept the new position, otherwise it will not move.

*Step 4*: besieging behavior. The scouting and calling behaviors make wolves stride forward to the direction of the optimal solution, which can speed up the convergence of WPA. Specifically, the process of besieging behavior is as follows. Firstly, one position between 1 and $A$ is randomly selected. Secondly, the variables of the wolf from ferocious wolves and scout wolves are replaced with those of the lead wolf in selected positions. Thirdly, if the objective function of the wolf in the new position is better than that in the old position, it will accept the new position, otherwise it will not move.

*Step 5*: updating wolves. The lead wolf, scout wolves, and ferocious wolves are reordered according to their objective functions, and the wolf with the best objective function is the new lead wolf. The $R$ wolves with the worst objective function will be reinitialized to ensure the diversity of wolves. If the program reaches the maximum number of iterations, the results of the lead wolf are output, otherwise return to *Step 2*.

### B. IWPA

In order to improve the stability and optimization performance of WPA, two strategies are proposed to improve WPA. The specific improvements are as follows.

1) Adaptive adjustment of step size. In the calling behavior of the traditional WPA, the step size ($k$ positions) of the ferocious wolves running to the lead wolf is fixed, which makes the loss function of traditional WPA appear jagged fitness landscape. In fact, the ferocious wolves that are far away from the lead wolf should run to the lead wolf in a large step size, and the ferocious wolves that are close to the lead wolf should run to the lead wolf in a small step size. In general, the optimal step size should be adjusted adaptively according to the objective function value of the ferocious wolf. In this paper, it assumes that the step size of the first ferocious wolf is 1, and that of the last ferocious wolf is $A-1$. The step size of the $r^{\text{th}}$ wolf is as follows:

$$S_r = \text{round}\left(\frac{(A-2)(f_r - f_1)}{f_V - f_1} + 1\right) \tag{13}$$

where $f_r (r = 1,2,...,V)$ is the objective function value of the $r^{\text{th}}$ wolf, and $V$ is the number of ferocious wolves. Specifically, the length of the control variables of the RVC model is $A$. For the $r^{\text{th}}$ ferocious wolf, it needs to exchange $S_r$ elements with the lead wolf.

2) Communication behavior between the ferocious wolves and the scout wolves. In the traditional WPA, the ferocious wolves only run in the direction of the lead wolf, and there is no communication between the ferocious wolves and the scout wolves. In order to enrich the diversity of solutions, this paper proposes the communication behavior between the ferocious wolves and the scout wolves before the besieging behavior. Specifically, the process of communication behavior is as follows. For the RVC model, the length of the control variables of the RVC model is $A$. The $A$ random numbers between 0 and 1 are obtained from Gaussian distribution. Secondly, the $r^{\text{th}}$ variables from a ferocious wolf and a scout wolf are exchanged if the $r^{\text{th}}$ random number is greater than $p$. It assumes that $p$ is the probability of the exchange. Thirdly, if the objective function of the wolf in the new position is better than that in the old position, it will accept the new position, otherwise it will not move.

In summary, the process of IWPA is shown in Fig. 2.

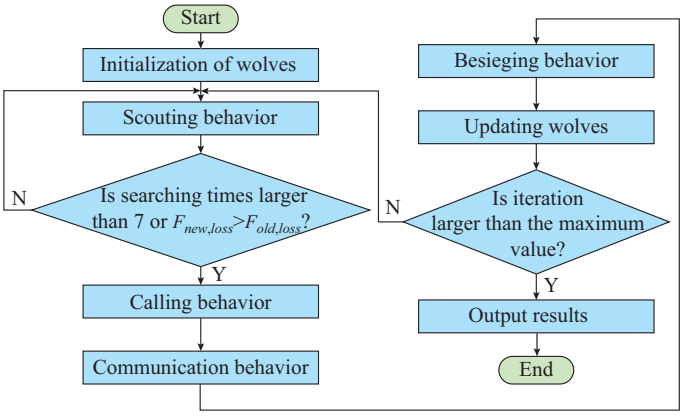


Fig. 2. Framework of IWPA.

## V. Case Study

### A. Scenario Generation for Renewable Energies and Loads

The smart meter dataset from low carbon London project [35] and the dataset of renewable energies from National Renewable Energy Laboratory (NREL) are used to verify the effectiveness of the proposed methods [36], [37]. After data cleaning, the wind and photovoltaic power profiles have 1460 samples with a resolution of 20 min, and the power load profiles have 483 samples with a resolution of 60 min. Nine neighboring wind farms, solar plants, and 32 neighboring load nodes of a distribution network are selected. Eighty

percent of the samples are used as the training set, and the remaining 20% is used as the test set. Along with these real data, the results of the day-ahead forecasting by the recurrent neural network are utilized to train IGAN.

The structures of IGAN for scenario generation of renewable energies and loads are similar. As shown in Fig. 3, the IGAN for generating wind power is used as an example to illustrate the structure and parameters. The input data of CNN is a 2-dimension matrix, so the input data of the discriminator are wind power profiles which are transformed into a matrix of 36×36 scales. The hidden layer is composed of one flatten layer and four convolutional layers whose activation functions are LeakyReLU. To alleviate the over-fitting, the Dropout layers are followed by the convolutional layers, and their values are 0.25. As a bridge between convolutional layers and dense layers, the flatten layer transforms multi-dimension data into a one-dimension vector. The output layer is a dense one where sigmoid is the activation function, and the output value of it is 1 or 0, which represents the input data are true or false, respectively. In terms of the generator, the random noises sampled from the Gaussian distribution are used as the input data. The hidden layer consists of one dense layer with 5184 neurons and 2 convolutional layers, and their activation functions are all ReLU. The output layer is a convolution layer whose activation function is the hyperbolic tangent. The IGAN generates multiple power profiles at the same time, which can capture the spatial correlation between multiple wind farms.

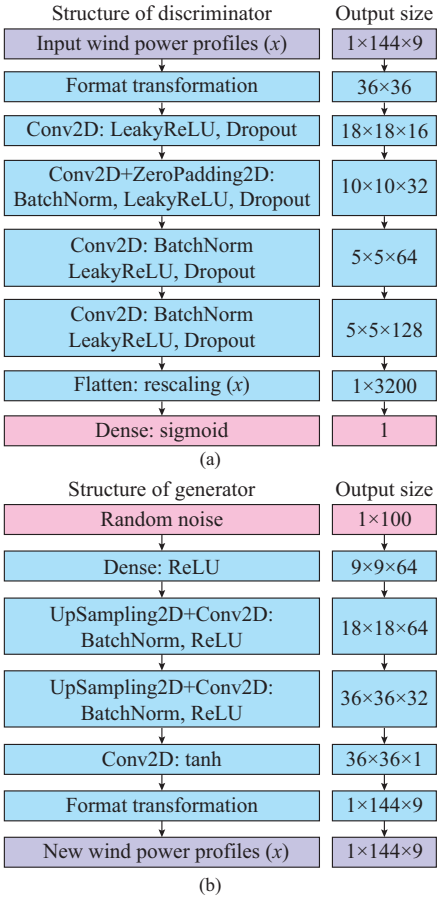


Fig. 3. Structure and parameters of IGAN. (a) Discriminator. (b) Generator.

The programs of generative networks for scenario generation are implemented in Anaconda navigator with Keras 2.2.2 and Tensorflow 1.10.0 library.

Figure 4 shows the training evolution of IGAN for generating wind power scenarios. The parameters of the generator are not optimal in the early training stage, and the scenarios generated by the generator are far from the real data, so the generated scenarios are easy to be recognized by the discriminator. When the number of iterations is more than 2000, the accuracy of the discriminator fluctuates up and down near 0.5, which indicates that the generator and the discriminator reach the Nash equilibrium, and the training procedure is stable. In order to ensure the convergence of the network, we choose the network after 5000 iterations to generate the scenarios.

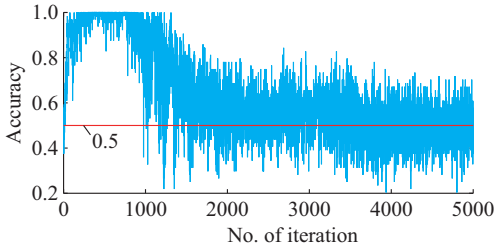


Fig. 4. Training evolution for IGAN on a wind dataset.

In order to prove that the scenarios generated by IGAN and the real scenarios have similar patterns, eight thousand random noises sampled from the Gaussian distribution are input into the generator, and a part of the generated samples and the real samples from the test set are shown in Fig. 5. Obviously, although the real samples in the test set are not used to train network, the shapes of generated samples for renewable energies and loads are very similar to those of the real samples from the test set, so that it is difficult for the naked eye to distinguish them. The IGAN can capture the nonlinear dynamic characteristics of real samples such as fluctuation, large valley, and fast ramps in power. Further, in order to compare the temporal correlation between the generated samples and the real samples, the autocorrelation functions are shown in Fig. 5. It is found that the trends of autocorrelation functions between the generated samples for renewable energies and the real samples are basically the same, which shows that the real samples generated by IGAN can reflect the temporal correlation of the real samples well.

The fluctuation of renewable energies and loads has a great influence on the operation of the power system. The power spectral densities (PSDs) represent the energy value of frequency components of time series, and are often used to represent the fluctuation components of loads and renewable energies at different frequencies. Figure 6 shows the PSDs of renewable energies and loads. It is obvious that the PSDs of generated samples closely resemble those of real samples from the test set, which indicates that IGAN can capture the frequency-domain characteristics of real samples well.

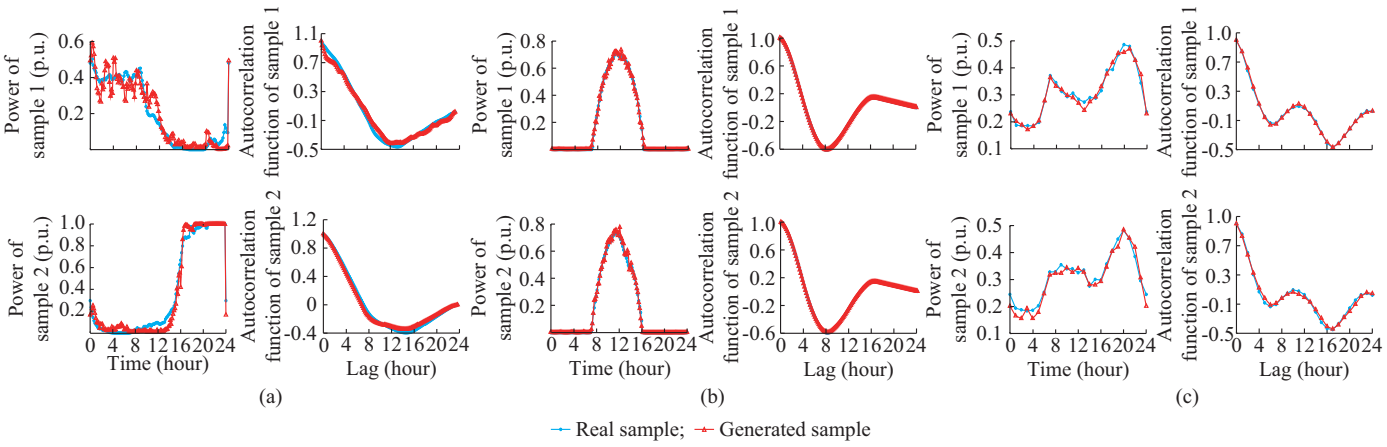


Fig. 5. Visualization of real samples from test set and generated samples from IGAN. (a) Wind power. (b) Photovoltaic power. (c) Power load.

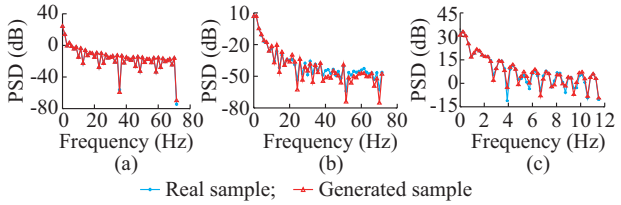


Fig. 6. PSDs of renewable energies and loads. (a) Wind power. (b) Photovoltaic power. (c) Power load.

To verify the performance of the IGAN, the traditional methods, e. g., VAE and GAN, are set up for comparison. Figure 7 shows the cumulative distribution functions (CDFs) of real samples and generated samples by three generative networks. It is found that the CDFs of samples generated by IGAN are closer to CDFs of real samples in comparison with VAE and GAN, both for loads and renewable energies. Moreover, IGAN shows the best performance of scenario generation of renewable energies and loads, which show that IGAN accurately capture the probability distribution characteristics of renewable energies and loads.

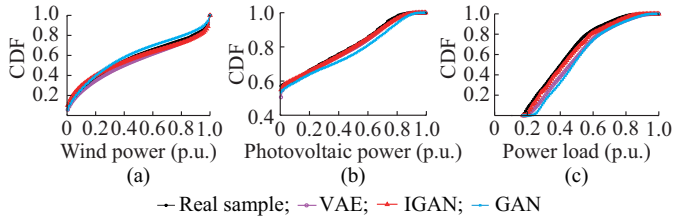


Fig. 7. CDF of renewable energies and loads. (a) Wind power. (b) Photovoltaic power. (c) Power load.

The changing pattern of the output power of nearby wind farms (solar plants) is similar, since their surrounding environment such as wind speed (light intensity) is similar. In the same way, most nodes of the distribution network are located in nearby areas, and they have similar electricity consumption habits, which lead to peak or valley in power load simultaneously. It is very important to consider the spatial correlation of renewable energies and loads for the economic operation and stability analysis of the distribution network.

To analyze whether IGAN can capture the spatial correlation of real samples, the correlation matrices of real samples and generated samples are calculated, respectively. Then, the correlation matrices of the generated samples are subtracted from those of the real samples, and their absolute values are calculated to obtain the error matrices. The visualization of the error matrices is shown in Figs. 8, 9, and 10.

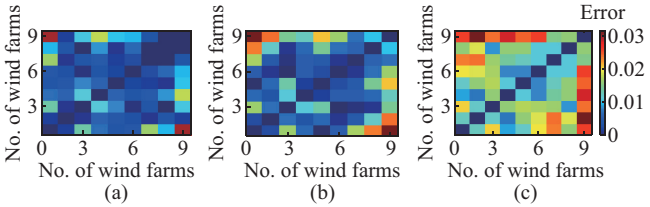


Fig. 8. Errors of wind farms. (a) IGAN. (b) GAN. (c) VAE.

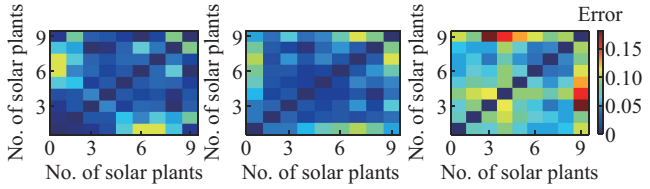


Fig. 9. Errors of solar plants. (a) IGAN. (b) GAN. (c) VAE.

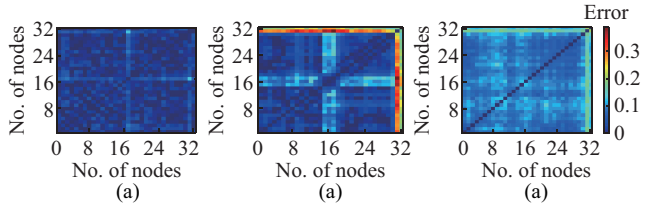


Fig. 10. Errors of power loads. (a) IGAN. (b) GAN. (c) VAE.

In terms of wind farms, most of the VAE errors are between 0.01 and 0.03. The GAN errors are smaller than VAE errors, and most of their errors are between 0.01 and 0.02. IGAN has the smallest errors, most of which are between 0 and 0.01. For solar plants, IGAN and GAN have similar performances, which are better than VAE. As far as power loads are concerned, the errors of GAN and IGAN mainly range from 0 to 0.05, and the performance of IGAN is slightly better than that of GAN. Most errors of VAE are between

0.05 and 0.3. In general, the performance of IGAN is better than those of GAN and VAE in terms of capturing spatial correlation, which shows that replacing the least squares loss function with the cross-entropy loss function can improve the performance of GAN.

### *B. RVC*

As shown in Fig. 11, the modified IEEE 33-bus radial distribution system is used to verify the effectiveness of the proposed method [38]. The voltage magnitude base is 12.66 kV. The tap position of the on-load tap changer includes 17 tap positions, and the transformer ratio ranges from $-8\times1.25\%$ to $8\times1.25\%$. The shunt capacitor banks are added at the nodes 10 and 14, the number of which is 15 banks. The capacity of each bank is 100 kvar. The SVC is added at node 17 and some micro-turbines are added at node 28. The reactive power of micro-turbines and SVC ranges from −1000 to 1000 kvar. Two solar plants are added at nodes 21 and 33. Two wind farms are added at nodes 7 and 25. The data of renewable energies and power loads of 32 nodes are generated by IGAN.

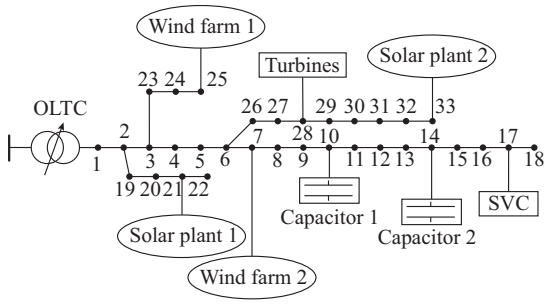


Fig. 11. Topology of modified IEEE 33-bus radial distribution system.

The number of generated scenarios should be large enough to adequately capture the uncertainties of renewable energies and loads. Therefore, eight thousand random noises sampled from Gaussian distribution are fed to the generator to obtain the scenarios of renewable energies and power load of nodes. To reduce the complexity of the algorithm, the *K*-means is used to reduce the number of similar scenarios. Specifically, $K$ needs to be set artificially. If $K$ is too small, the new scenarios cannot reflect enough information about the original ones. On the contrary, if $K$ is too large, the proposed method will become very complex and consume a lot of computing time. In this paper, the sum of the squared error (SSE) is used to determine the optimal $K$. The SSE of renewable energies and power loads at different $K$ are shown in Fig. 12.

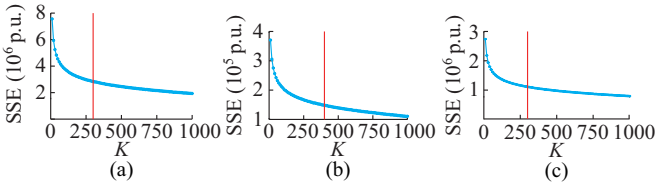


Fig. 12. SSE of renewable energies and loads. (a) Wind power. (b) Photovoltaic power. (c) Power load.

With the increase of $K$, the number of samples in each group becomes smaller, and each sample is closer to the centroids, resulting in SSE becoming smaller. When $K$ is less than the optimal value, the increase of $K$ greatly reduces the distance between the centroid and each sample in each group. Therefore, SSE decreases rapidly in the early stage. When $K$ is greater than the optimal value, the increase of $K$ has little effect on the decrease in distance. Consequently, SSE decreases slowly in the late stage. In general, the relationship between SSE and $K$ is like a visual "elbow", which is the optimal number of scenarios. As we can see, at $K=300$, the curve begins to flatten significantly, so three hundred typical scenarios with different forecasting errors for renewable energies and loads are selected for RVC in this paper. Furthermore, Fig. 13 shows the CPFs of the real samples and the generated samples after reduction. Obviously, the 300 generated samples accurately capture the probability distribution characteristics of the real samples, which show that the 300 samples selected by *K*-means can be used in robust optimization.

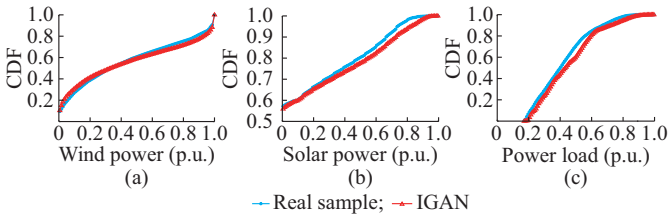


Fig. 13. CDFs of real samples and 300 generated samples. (a) Wind power. (b) Photovoltaic power. (c) Power load.

To compare the performance of DVC and RVC models, it assumes that the upper limit of the voltage is 1.05 p.u. and the lower limit of voltage is 0.95 p.u. for generic nodes.

Table I, Table II, and Fig. 14 show the voltage and power loss of the DVC and RVC model in different scenarios. In the solution of the DVC model, the turbines and SVC output a lot of reactive power, which reduces the power loss and raises the voltages. In the normal scenario, the solution of the DVC model can control the voltages within the limit and the power loss is very small. However, the solution of the DVC model is not suitable for extreme scenarios (e.g., the loads are small and the output power of renewable energies is large), in which the voltages of some nodes (e.g., node 17 and 18) are greater than 1.05 p.u. In the solution of the DVC model, the gas turbine and SVC absorb a lot of reactive power, which increases the power loss and reduces the voltages. Although the solution of the RVC model results in the power loss in the normal scenario larger than that of DVC model, it can ensure that the voltage of each node in the extreme scenarios does not exceed the upper limit.

TABLE I
VOLTAGE AND POWER LOSSES IN DIFFERENT SCENARIOS

| Scenario | DVC | | RVC | |
|---|---|---|---|---|
| | Loss (kW) | Voltage (p.u.) | Loss (kW) | Voltage (p.u.) |
| Normal | 43.49 | [1.02, 1.05] | 80.36 | [0.99, 1.05] |
| Extreme | 31.01 | [0.93, 1.05] | 52.74 | [1.01, 1.05] |

TABLE II
PARAMETERS OF EACH EQUIPMENT

| Model | Turbine (kvar) | SVC (kvar) | Capacitor 1 (kvar) | Capacitor 2 (kvar) |
|---|---|---|---|---|
| DVC | 787.41 | 226.30 | 400 | 300 |
| RVC | –256.23 | –246.62 | 600 | 900 |

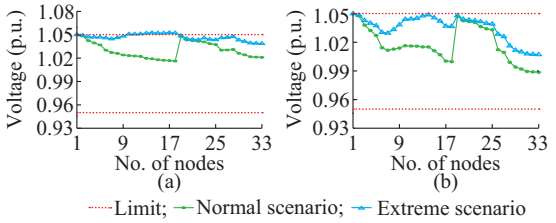


Fig. 14. Voltage amplitude of each node in different scenarios. (a) DVC. (b) RVC.

Similarly, there may be another extreme scenario (e.g., the loads are large and the output power of renewable energies are small) where the voltage of some nodes exceeds the lower limit. As shown in Table III, Table IV, and Fig. 15, the RVC model adjusts the state of the equipment, so that the voltage can always be safe in both normal and extreme scenarios.

TABLE III
VOLTAGE AND POWER LOSSES IN DIFFERENT SCENARIOS

| Scenarios | DVC | | RVC | |
|---|---|---|---|---|
| | Loss (kW) | Voltage (p.u.) | Loss (kW) | Voltage (p.u.) |
| Normal | 43.49 | [1.02, 1.05] | 53.04 | [1.01, 1.05] |
| Extreme | 173.67 | [0.93, 1.05] | 168.21 | [0.95, 1.05] |

TABLE IV
PARAMETERS OF EACH EQUIPMENT

| Model | Turbine (kvar) | SVC (kvar) | Capacitor 1 (kvar) | Capacitor 2 (kvar) |
|---|---|---|---|---|
| DVC | 787.41 | 226.30 | 400 | 300 |
| RVC | 324.26 | 84.40 | 1100 | 300 |

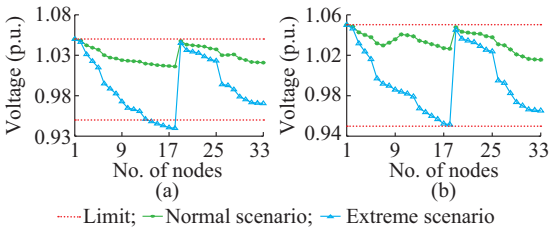


Fig. 15. Voltage amplitude of each node in different scenarios. (a) DVC. (b) RVC.

To analyze the importance of the generated scenario quality for the RVC model, Fig. 16 shows the results of the RVC model considering the uncertainties of renewable energies and loads based on the traditional method (e. g. VAE) and IGAN.

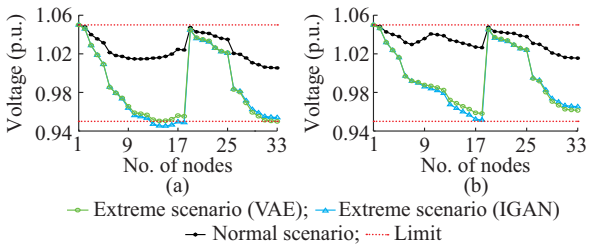


Fig. 16. Voltage amplitude of each node in different scenarios. (a) VAE. (b) IGAN.

Obviously, the solution of extreme scenarios from VAE cannot guarantee that the voltage is not less than the lower limit of extreme scenarios from IGAN, while it can ensure the safe operation of the power system in any scenario. VAE prefers to generate simple data and avoid extreme scenarios with a small number in the training set [13]. Therefore, the errors between normal scenarios and extreme scenarios generated by VAE are smaller than the real errors. In this case, it can be considered that the extreme scenario generated by IGAN is more suitable for RVC than the extreme scenario generated by VAE, because the probability distribution of the scenarios generated by IGAN is very close to the real scenarios, which have been proven in Section V-A.

To further compare the performance of DVC and RVC models in different scenarios, the IGAN is used to generate 2000 scenarios, and calculate the power flow and voltage of these scenarios. Then, the voltages and power loss of each scenario are caculated as shown in Table V-A.

TABLE V
STATISTICAL RESULTS OF VOLTAGE AND POWER LOSSES

| Model | No. of insecure scenarios | Percentage of insecure scenarios (%) | Mean of power loss (kW) |
|---|---|---|---|
| DVC | 115 | 5.75 | 50.95 |
| RVC | 0 | 0 | 57.31 |

It is obvious that the voltage will exceed the limit in some scenarios if the results of the DVC model are used. In contrast, the results of the RVC model can ensure that the voltages are safe in all scenarios, but it comes at the cost of power loss.

### C. Performance Tests for IWPA

In addition to the proposed IWPA, the WPA, GA, ABC, and ICA are also set up for comparison. Stability, speed of convergence, and accuracy are used to evaluate the performance of these algorithms. In order to ensure a fair benchmark, many experiments are carried out to find the best structure and hyper-parameters of each method. The best parameters of IWPA are shown as follows.

The wolf pack consists of 50 wolves, which include 25 scout wolves and 25 ferocious wolves. The $h$ is equal to 1 in scouting behavior. The step size is adaptive for IWPA. Besides, the $p$ is equal to 0.7 in communication behavior. The maximum numbers of iterations are 100.

In order to fully test the performance of the algorithm, each algorithm is tested 50 times independently, and the re-

sults are shown in Table VI and Fig. 17.

TABLE VI
STATISTICAL RESULTS OF EACH METHOD

| Method | Min loss (kW) | Max loss (kW) | Mean loss (kW) | Standard deviation (kW) | Iterative time for convergence (s) |
|---|---|---|---|---|---|
| IWPA | 121.89 | 122.16 | 121.93 | 0.08 | 37.85 |
| WPA | 122.93 | 132.47 | 126.12 | 1.91 | 17.33 |
| ABC | 122.43 | 135.16 | 125.92 | 3.15 | 49.35 |
| GA | 121.90 | 125.04 | 122.51 | 0.75 | 43.05 |
| ICA | 121.92 | 122.68 | 122.06 | 0.16 | 42.65 |

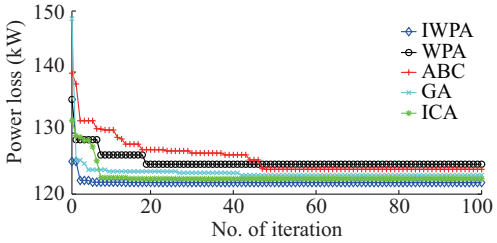


Fig. 17. Training evolution of each method.

For the speed of convergence, ABC has the worst convergence performance, and convergence requires about 49 iterations. Although the convergence speed of WPA is faster than that of IWPA, its accuracy is not high, which shows that WPA is easy to fall into the local optimum. Besides, the convergence speed of IWPA is faster than those of GA and ICA. For stability, IWPA is better than that of other methods by comparing the standard deviation. The stability of GA and ICA is similar. The standard deviation of ABC and WPA is large, which indicates that the result of the optimization is not very stable. For accuracy, the optimal solution, the worst solution, and the average solution of IWPA are better than other methods. In general, IWPA shows better performance than traditional methods in terms of convergence speed, accuracy, and stability for RVC.

## VI. DISCUSSION

The objective of this paper is to propose a new method based on IGAN and IWPA to guarantee the safe operation of the distribution network in any scenario. In this paper, the effectiveness of the proposed IGAN is tested on the smart meter dataset from low carbon London project and the dataset of renewable energies from NREL including wind farms, solar plants, and power loads. Furthermore, IGAN can be used to generate scenarios for renewable energies and loads from different places by adjusting the structure and parameters. Besides, the IWPA can be generalized to solve other optimization problems such as reactive power optimization for the distribution network.

## VII. CONCLUSION

In this paper, an RVC model is proposed to cope with the uncertainties of renewable energies and loads via a novel GAN. Two strategies are proposed to improve the traditional GAN, since the data it produces have low quality and the training is not stable. Furthermore, a new IWPA is presented to solve the formulated RVC model. Based on simulation results, the conclusions are as follows.

1) IGAN can accurately capture the probability distribution characteristics and dynamic nonlinear characteristics (e. g., fluctuation and temporal-spatial correlation) of renewable energies and loads, which makes the scenarios generated by IGAN more suitable for RVC than those generated by traditional methods, e.g., traditional GAN and VAE.

2) If the error between the actual value and the predicted value is large, the solution of the DVC model may make the voltage exceed the limit. In contrast, the results of the RVC model can ensure that the voltages are safe in all scenarios but it comes at the cost of power loss.

3) After independent repeated tests, the results show that the IWPA has better performance than traditional methods (e. g., the GA, ABC, WPA, and ICA) in terms of convergence speed, accuracy, and stability for RVC.

For future work, some other generative networks may also be suitable for robust optimization in the distribution network. How to apply these generative networks to the optimization of distribution network deserves further study.

## REFERENCES

[1] S. Xia, S. Bu, X. Luo *et al*., "An autonomous real-time charging strategy for plug-in electric vehicles to regulate frequency of distribution system with fluctuating wind generation," *IEEE Transactions on Sustainable Energy*, vol. 9, no. 2, pp. 511-524, Apr. 2018.
[2] M. Li, Z. Lin, T. Ji *et al*., "Risk constrained stochastic economic dispatch considering dependence of multiple wind farms using pair-copula," *Applied Energy*, vol. 226, pp. 967-978, Sept. 2018.
[3] M. Jiang, Q. Guo, H. Sun *et al*., "Day-ahead voltage scheduling method based on a two-stage robust optimisation for VSC-HVDC connected wind farms," *IET Renewable Power Generation*, vol. 12, no. 13, pp. 1470-1477, Sept. 2018.
[4] N. Daratha, B. Das, and J. Sharma, "Robust voltage regulation in unbalanced radial distribution system under uncertainty of distributed generation and loads," *International Journal of Electrical Power & Energy Systems*, vol. 73, pp. 516-527, Dec. 2015.
[5] T. Ding, Q. Yang, Y. Yang *et al*., "A data-driven stochastic reactive power optimization considering uncertainties in active distribution networks and decomposition method," *IEEE Transactions on Smart Grid*, vol. 9, no. 5, pp. 4994-5004, Sept. 2018.
[6] F. Alismail, P. Xiong, and C. Singh, "Optimal wind farm allocation in multi-area power systems using distributionally robust optimization approach," *IEEE Transactions on Power Systems*, vol. 3, no. 1, pp. 536-544, Jan. 2018.
[7] H. Baghaee, M. Mirsalim, G. Gharehpetian *et al*., "Fuzzy unscented transform for uncertainty quantification of correlated wind/PV microgrids: possibilistic-probabilistic power flow based on RBFNNs," *IET Renewable Power Generation*, vol. 11, no. 6, pp. 867-877, May 2017.
[8] H. Baghaee, M. Mirsalim, G. Gharehpetian *et al*., "Application of RBF neural networks and unscented transformation in probabilistic power-flow of microgrids including correlated wind/PV units and plug-in hybrid electric vehicles," *Simulation Modelling Practice and Theory*, vol. 72, pp. 51-68, Mar. 2017.
[9] Y. Liu, C. Jiang, J. Shen *et al*., "Coordination of hydro units with wind power generation using interval optimization," *IEEE Transactions on Sustainable Energy*, vol. 6, no. 2, pp. 443-453, Apr. 2015.
[10] B. Jeddi, V. Vahidinasab, P. Ramezanpour *et al*., "Robust optimization framework for dynamic distributed energy resources planning in distribution networks," *International Journal of Electrical Power & Energy Systems*, vol. 110, pp. 419-433, Sept. 2019.
[11] M. Ghafouri, U. Karaagac, H. Karimi *et al*., "Robust subsynchronous interaction damping controller for DFIG-based wind farms," *Journal of Modern Power Systems and Clean Energy*, vol. 7, no. 6, pp. 1663-

1674, Nov. 2019.
[12] J. Toubeau, J. Bottieau, F. Vallee *et al*., "Deep learning-based multivariate probabilistic forecasting for short-term scheduling in power markets," *IEEE Transactions on Power Systems*, vol. 34, no. 2, pp. 1203-1215, Mar. 2019.
[13] W. Hu, H. Zhang, Y. Dong *et al*., "Short-term optimal operation of hydro-wind-solar hybrid system with improved generative adversarial networks," *Applied Energy*, vol. 250, pp. 389-403, Sept. 2019.
[14] Z. Pan, J. Wang, W. Liao *et al*., "Data-driven EV load profiles generation using a variational auto-encoder," *Energies*, vol. 12, no. 5, pp. 849-863, Mar. 2019.
[15] Y. Chen, Y. Wang, D. Kirschen *et al*., "Model-free renewable scenario generation using generative adversarial networks," *IEEE Transactions on Power Systems*, vol. 33, no. 3, pp. 3265-3275, May 2018.
[16] X. Mao, Q. Li, H. Xie *et al*., "Least squares generative adversarial networks," in *Proceedings of 2017 IEEE International Conference on Computer Vision*, Venice, Italy, Oct. 2017, pp. 2813-2821.
[17] O. Alsac, J. Bright, M. Prais *et al*., "Further developments in LP-based optimal power flow," *IEEE Transactions on Power Systems*, vol. 5, no. 3, pp. 697-711, Aug. 1990.
[18] K. Aoki, M. Fan, and A. Nishikori, "Optimal var planning by approximation method for recursive mixed-integer linear programming," *IEEE Transactions on Power Systems*, vol. 3, no. 4, pp. 1741-1747, Nov. 1988.
[19] T. Ding, S. Liu, and W. Yuan, "A two-stage robust reactive power optimization considering uncertain wind power integration in active distribution networks," *IEEE Transactions on Sustainable Energy*, vol. 7, no. 1, pp. 301-311, Jan. 2016.
[20] R. Jabr, I. Dzafic, and I. Huseinagic, "Real time optimal reconfiguration of multiphase active distribution networks," *IEEE Transactions on Smart Grid*, vol. 9, no. 6, pp. 6829-6839, Nov. 2018.
[21] T. Mareda, L. Gaudard, F. Romerio *et al*., "A parametric genetic algorithm approach to assess complementary options of large scale windsolar coupling," *IEEE/CAA Journal of Automatica Sinica*, vol. 4, no. 2, pp. 260-272, Apr. 2017.
[22] C. Liu, J. Wang, M. Zhou *et al*., "Reconfiguration of virtual cellular manufacturing systems via improved imperialist competitive approach," *IEEE Transactions on Automation Science and Engineering*, vol. 16, no. 3, pp. 1301-1314, Jul. 2019.
[23] G. Tian, Y. Ren, Y. Feng *et al*., "Modeling and planning for dual-objective selective disassembly using and/or graph and discrete artificial bee colony," *IEEE Transactions on Industrial Informatics*, vol. 15, no. 4, pp. 2456-2468, Apr. 2019.
[24] K. Wang, C. Gou, Y. Duan *et al*., "Generative adversarial networks: introduction and outlook," *IEEE/CAA Journal of Automatica Sinica*, vol. 4, no. 4, pp. 588-598, Sept. 2017.
[25] L. Chen, X. Hu, W. Tian *et al*., "Parallel planning: a new motion planning framework for autonomous driving," *IEEE/CAA Journal of Automatica Sinica*, vol. 6, no. 1, pp. 236-246, Jan. 2019.
[26] P. Xiang, L. Wang, F. Wu *et al*., "Single-image de-raining with feature-supervised generative adversarial network," *IEEE Signal Processing Letters*, vol. 26, no. 5, pp. 650-654, May 2019.
[27] J. Hertz, A. Krogh, B. Lautrup *et al*., "Nonlinear backpropagation: doing backpropagation without derivatives of the activation function," *IEEE Transactions on Neural Networks*, vol. 8, no. 6, pp. 1321-1327, Nov. 1997.
[28] G. Yao, T. Lei, and J. Zhong, "A review of convolutional-neural-network-based action recognition," *Pattern Recognition Letters*, vol. 118, pp. 14-22, Feb. 2019.
[29] A. Radford, L. Metz, and S. Chintala, "Unsupervised representation learning with deep convolutional generative adversarial networks," in *Proceedings of 4th International Conference on Learning Representations*, San Juan, USA, May 2016, pp. 1-16.
[30] J. Springenberg, A. Dosovitskiy, and T. Brox, "Striving for simplicity: the all convolutional net," in *Proceedings of 3th International Conference on Learning Representations*, San Diego, USA, May 2015, pp. 1-14.
[31] S. Ioffe and C. Szegedy, "Batch normalization: accelerating deep network training by reducing internal covariate shift," in *Proceedings of 32nd International Conference on Machine Learning*, Lille, France, Jul. 2015, pp. 448-456.
[32] B. Xu, N. Wang, T. Chen *et al*. (2015, Feb.). Empirical evaluation of rectified activations in convolutional network. [Online]. Available: https://arxiv.org/abs/1505.00853
[33] H. Wu and F. Zhang, "Wolf pack algorithm for unconstrained global optimization," *Mathematical Problems in Engineering*, vol. 2014, pp. 1-17, Mar. 2014.
[34] L. Zhang, L. Zhang, S. Liu *et al*., "Three-dimensional underwater path planning based on modified wolf pack algorithm," *IEEE Access*, vol. 5, pp. 22783-22795, Oct. 2017.
[35] UK Power Networks. (2015, Jun.). Low carbon london project. [Online]. Available: https://data. london. gov. uk/dataset/smartmeter-energy-use-data-in-london-households
[36] National Renewable Energy Laboratory. (2012, Nov.). Solar integration national dataset toolkit. [Online]. Available: https://www.nrel.gov/grid/sind-toolkit.html
[37] C. Draxl, A. Clifton, B. Hodge *et al*., "The wind integration national dataset (WIND) toolkit," *Applied Energy*, vol. 151, pp. 355-366, Aug. 2015.
[38] M. Baran and F. Wu, "Network reconfiguration in distribution systems for loss reduction and load balancing," *IEEE Transactions on Power Delivery*, vol. 4, no. 2, pp. 1401-1407, Apr. 1989.

**Qianyu Zhao** received the B.S. and M.S. degrees in electrical engineering and control science and engineering from Tiangong University, Tianjin, China, in 2012 and 2015, respectively, and the Ph.D. degree in electrical engineering from Tianjin University, Tianjin, China, in 2020. She is currently an Assistant Professor with the School of Electrical and Information Engineering, Tianjin University. Her research interests include planning, assessment of energy storage and distributed generation, uncertainty analysis of distribution networks.

**Wenlong Liao** received the B.S. degree in electrical engineering from China Agricultural University, Beijing, China, in 2017. He is currently pursuing the M.S degree in electrical engineering in Tianjin University, Tianjin, China. His current research interests include smart grid, machine learning, and renewable energy.

**Shouxiang Wang** received the B.S. and M.S. degrees in electrical engineering from Shandong University of Technology, Jinan, China, in 1995 and 1998, respectively, and the Ph.D. degree in electrical engineering from Tianjin University, Tianjin, China, in 2001. He is currently a Professor with the School of Electrical and Information Engineering, and Deputy Director of Key Laboratory of Smart Grid of Ministry of Education, Tianjin University. His main research interests are distributed generation, microgrid, and smart distribution system.

**Jayakrishnan Radhakrishna Pillai** received the M.Tech. degree in power systems from the National Institute of Technology, Calicut, India, in 2005, the M.Sc. degree in sustainable energy systems from the University of Edinburgh, Edinburgh, U.K., in 2007, and the Ph.D. degree in power systems from Aalborg University, Aalborg, Denmark, in 2011. He is currently an Associate Professor with the Department of Energy Technology, Aalborg University. His current research interests include distribution system analysis, grid integration of electric vehicles and distributed energy resource, smart grids, and intelligent energy systems.